Towards a Single Solution for Polyp Detection, Localization and Segmentation in Colonoscopy Images

Willem Dijkstra[1], André Sobiecki[1,2], Jorge Bernal[3] and Alexandru C. Telea[2]
[1]*Bernoulli Institute, University of Groningen, The Netherlands*
[2]*ZiuZ Visual Intelligence, Gorredijk, The Netherlands*
[3]*Image Sequence Evaluation laboratory, Computer Vision Center and Universitat Autónoma de Barcelona, Spain*

Keywords: Machine Learning, CNNs, Polyp Detection, Polyp Segmentation, Colonoscopy.

Abstract: Colorectal cancer is one of the main causes of cancer death worldwide. Early detection of its precursor lesion, the polyp, is key to ensure patient survival. Despite its gold standard status, colonoscopy presents some drawbacks such as polyp misses. While several computer-based solutions in this direction have been proposed, there is no available solution tackling lesion detection, localization and segmentation at once. We present in this paper a one-shot solution to characterize polyps in colonoscopy images. Our method uses a fully convolutional neural network model for semantic segmentation. Next, we apply transfer learning to provide detection and localization. We tested our method on several public datasets showing promising results, including compliance with technical and clinical requirements needed for an efficient deployment in the exploration room.

1 INTRODUCTION

Colorectal cancer (CRC) is the second leading cause of cancer death in the USA and is estimated to have caused 50260 deaths in 2017 only, according to American Cancer Society (Siegel et al., 2017). Most CRCs develop from adenomatous polyps that can appear anywhere in the colon. Early detection and removal of polyps is of great significance when performing colonoscopy for prevention and timely treatment of CRC. However, the average polyp miss-rate in colonoscopy is estimated to be up to 25% (Leufkens et al., 2012). Missing polyps can lead to a late diagnosis of CRC with low survival rates (Rabeneck et al., 2003).

Computational systems can assist clinicians in polyp detection and thus decrease the polyp miss-rate. However, automatic polyp detection in colonoscopy videos is very challenging due to high variations in polyp appearance (size, colour, shape, texture) and the presence of other endoluminal scene structures (*e.g.*, colon walls, specular highlights and air bubbles).

In the past few decades, many algorithms have been developed to automate the detection, localization, and segmentation of polyps in colonoscopy images. Significant progress has been made in recent years. End-to-end learning methods seem to give the best results for automatic detection and localization of polyps (Bernal et al., 2017). Polyp segmentation has not attracted yet the same level of attention. However, segmentation has an advantage over detection and localization, as it also gives information about a polyp's shape and it could be used as a preliminary stage for in-vivo diagnosis.

We propose in this paper to use polyp segmentation as the main output from which polyp detection and localization can be derived. Our proposal is based on a convolutional neural network (CNN), in our case a residual network (ResNet50). We validate our method against several publicly available datasets for detection, localization and/or segmentation.

2 RELATED WORK

Existing algorithms for polyp characterization can be grouped in three categories (Bernal et al., 2017): ***hand-crafted features***, ***end-to-end learning***, and ***hybrid***, as follows. For each method class, we also list its comparative advantages and limitations.

Dijkstra, W., Sobiecki, A., Bernal, J. and Telea, A.
Towards a Single Solution for Polyp Detection, Localization and Segmentation in Colonoscopy Images.
DOI: 10.5220/0007694906160625
In *Proceedings of the 14th International Joint Conference on Computer Vision, Imaging and Computer Graphics Theory and Applications (VISIGRAPP 2019)*, pages 616-625
ISBN: 978-989-758-354-4

2.1 Hand-crafted Features

These methods are based on the extraction of features (based on shape, color, or texture) from the image that are explicitly defined by the user. Such features are next fed into a ML system that provides the desired inference (*e.g.*, classification or segmentation) based on a mix of user-specified and learned parameter values.

Advantages:

- no (large) training dataset is needed;
- if strongly discriminating features of an object are explicitly known (e.g. colour or shape), extracting the object is relatively easy and computationally efficient;

Disadvantages:

- specialist experts are needed for feature design;
- no single hand-crafted feature might solve the problem, so multiple hand-crafted features are typically needed. Finding the right mix and settings of such a feature set is challenging.

2.2 End-to-end Learning

End-to-end learning systems, such as neural networks, merge all intermediate stages present in classical ML systems, such as data preprocessing, feature engineering and extraction, and actual inference. Inference is done exclusively based on (internal) parameters which are learned from a training set.

Advantages:

- once correctly set up (trained), such systems can deliver very high accuracy at high speed, and with limited or no user intervention;

Disadvantages:

- large amounts of (labeled) training data is needed;
- little control exists over how the system learns to infer;
- training can be computationally expensive;
- understanding how these systems infer can be hard.

2.3 Hybrid Approaches

Hybrid methods combine hand-crafted features (mainly to provide a first rough object detection) with end-to-end learning (to discriminate those detected objects likely to be polyps).

Advantages:

- aim to get the best of 'both worlds' (hand-crafted features and end-to-end learning), thus requiring less training effort;

Disadvantages:

- the amount of required training data can still be large;
- parameter tuning can be hard.

Following the above, we have produced a survey that organizes methods for polyp detection, localization, and segmentation along the aforementioned three method classes. Tables 1 and 2 show the identified methods. For each method, we indicate the types of used features, ML technique it is based on, and amount of data the method was tested with. Next, we rank each method along two desirable criteria – validation (**V**) and reproducibility (**R**) – using a 5-point ordinal Likert scale ($--, -, +/-, +, ++$). As visible from this survey, no single method scores well on both criteria for all three tasks of polyp detection, localization, and segmentation.

3 PROPOSED METHOD

Architecture: For polyp semantic segmentation, we propose to use Fully Convolutional Networks (FCNs), implemented with Keras and TensorFlow. In traditional CNNs, an operating block would compute from am input x an output $F(x)$ which is a completely new representation that does not keep any information about the input x. In contrast, FCNs compute a 'delta' or slight change $x + F(x)$ of the original input x (Fig. 1). It is proved that training

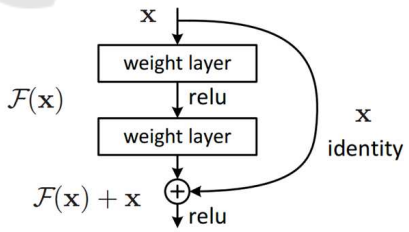

Figure 1: A residual block (He et al., 2016).

this form of networks (FCNs) is easier than training general CNNs. Also, FCNs resolve better the issue of degrading accuracy (He et al., 2016). We use ResNet50 which specifically is a residual network which consists of 50 layers. We next outline the optimization and training of the network. Table 3 gives an overview of all relevant parameters.

Table 1: Comparison of different methods for polyp detection. **V** = Validation and **R** = Reproducibility.

POLYP DETECTION		**Hand-crafted features**			
Method	Descriptors Features	Classification	Database	**V**	**R**
(Tjoa and Krishnan, 2003)	Texture spectrum, color histograms	NN	12 images (no-polyp) and 54 images (polyp)	+/-	-
(Dhandra et al., 2006)	Number of regions after morphological watershed segmentation	-	50 images (no-polyp) and 50 images (polyps)	+/-	+/-
(Hwang et al., 2007)	Curve direction, curvature, edge distance, intensity	-	27 images (polyps)	-	-
(Alexandre et al., 2007)	RGB-values and coordinates of each pixel	SVM	35 images	+	-
(Alexandre et al., 2008)	Color and position features	SVM with REF kernel	4600 images from 35 videos	+	+
(Karargyris and Bourbakis, 2009)	Curvature features	Based on segmentation from log-Gabor and SUSAM	40 images without polyp, 10 images with polyp	+	+/-
(Hwang and Celebi, 2010)	Geometric feature	Rule based	128 images	+/-	-
(Eskandari et al., 2012)	Geometric feature	Rule based	18 images	+/-	-
(Wang et al., 2014)	Edge profiles	SVM, GLM	1513 images	++	+/-
(Zhou et al., 2014)	Statistical information	SVM	359 VCE frames 294 for training and 65 for testing (performance)	-	-
(Mamonov et al., 2014)	Radios best fit ball	Binary classifier	Total 18968 images with 18738 images without and 230 images with polyps	+/-	-
(Iakovidis and Koulaouzidis, 2014)	Color features around SURF points	SVM	137 images	+	-
(Ratheesh et al., 2016)	HSV thresholding, Markovian Random Field	SVM	10 Videos of each 2100 frames	+/-	-
		End-to-end learning			
(Tajbakhsh et al., 2015)	Learned features (CNN)	Voting	7,000 frames with polyps and 28,000 frames with no polyps	++	+/-
(Yu et al., 2017)	Learning features (3D - FCN)	-	ASU-Mayo	++	+/-
(OUS) (Bernal et al., 2017)	Learning features (CNN)	Sliding-window strategy	CVC-CLINIC, ETIS-LARIB, ASU-Mayo	++	+
(CUMED) (Bernal et al., 2017)	Learning features (CNN)	Pixel-wise	CVC-CLINIC, ETIS-LARIB, ASU-Mayo	++	+
		Hybrid methods			
(Maroulis et al., 2003)	GLCM-features and discrete wavelet transform in CoLD	ANN	-	+	-
(Karkanis et al., 2003)	Color wavelet covariance (CWC)	-	2 images (no-polyp) and 4 images (polyp)	+/-	-
(Magoulas et al., 2004)	GLCM-features	NN	-	+/-	-
(Iakovidis et al., 2005)	Color wavelet covariance (CWC)	LDA	1380 images	+	+/-
(Silva et al., 2014) (ETIS-LARIB) (Bernal et al., 2017)	ROI, based on shape and size features; hough transform (detection), Texture analysis	Ad-hoc classifier (boosting-based learning process (co-ocurrence matrix))	CVC-CLINIC, ASU-Mayo	++	+
POLYP SEGMENTATION		**Hand-crafted features**			
Method	Descriptors Features	Classification	Database	**V**	**R**
(Ganz et al., 2012) (Shape-UCM)	Boundary detection and segmentation	-	Two datasets (58 images for training, 87 images for testing)	+	-
		End-to-end learning			
(Vázquez et al., 2017)	Learned features (CNN)	Tune an existing classifier	CVC-ColonDB, CVC-ClinicDB, CVC-EndoSceneStill	++	+
(Brandao et al., 2017)	Learned features (CNN)	Tune an existing classifier	CVC-ClinicDB, ETIS-LARIB, ASU-Mayo	++	+

Optimizer: To optimize our network, we use the well-known Adam optimizer (Kingma and Ba, 2014). Adam is an optimizer that converges fast due to using a larger effective step size. The disadvantage with this optimization algorithm, however, is that it is computational expensive as it uses moving averages of the parameters.

Table 2: Comparison of different methods for polyp localization and segmentation. **V** = Validation and **R** = Reproducibility.

POLYP LOCALIZATION		**Hand-crafted features**			
Method	Descriptors Features	Classification	Database	**V**	**R**
(Park et al., 2012)	Eigen-space representation	CRF	35 videos (1.2-25 million frames)	+	+/-
(Tajbakhsh et al., 2014)	ID discrete cosine transform (DCT)	Random Forest classifier	CVC-ColonDB	++	+
(Bernal et al., 2015) (CVC-CLINIC) (Bernal et al., 2017)	Protruding surfaces, boundaries defined from intensity valleys detection	Continuity, completeness, concavity and robustness against spurious structures	CVC-CLINIC, ETIS-LARIB, ASU-Mayo	++	+
(Tarik et al., 2016)	ROI's based on Gaussian Mixture Model, Esperance Maximization	-	100 images of different types of polyps	+	-
		End-to-end learning			
(SNU) (Bernal et al., 2017)	Learning features (CNN)	Binary classifier	CVC-CLINIC, ETIS-LARIB, ASU-Mayo	++	+
(UNS-UCLAN) (Bernal et al., 2017)	Learning features (CNN)	Multilayer perceptron (MLP)	CVC-CLINIC	++	+
		Hybrid methods			
(Tajbakhsh et al., 2016) (ASU) (Bernal et al., 2017)	Geometric features, Ensemble of CNNs	Voting	ETIS-LARIB	++	+/-
- (PLS) (Bernal et al., 2017)	Global image features (detection), Sequence of preprocessing filters (localization)	Means of the maximum values in the energy map computed using the elliptical shape of the polyp's usual appearance	CVC-CLINIC, ASU-Mayo, ETIS-LARIB	++	+/-

Table 3: Training parameters used by our network.

Parameter	**Value**
Maximum epochs	250
Learning rate base	0.0001
Learning rate power	0.9
Batch size	5
Batchnorm momentum	0.9

Early Stopping: We set the maximum number of training epochs to $max\_epochs = 250$. However, in order to prevent the network from overfitting, we use *early stopping*. This technique monitors a specified metric and stops network training when its loss is not decreasing. Early stopping requires two parameters: (1) the minimum change in the monitored metric that qualifies as an improvement (min_delta) and (2) the number of epochs with no improvement after which training is stopped ($patience$). In our experiments, we set the metric to be monitored with $min\_delta = 0.0001$ and $patience = 25$.

Learning Rate: During training, we slowly decrease the learning rate lr as

$$lr = lr\_base \cdot \left(1 - \frac{current\_epoch}{max\_epochs}\right)^{lr\_power} \quad (1)$$

where lr_base, the starting learning rate, is set to 0.0001 and $lr\_power = 0.9$.

Data Augmentation: We propose to apply data augmentation as previous studies show that it leads to better results in terms of mean Jaccard and mean global accuracy (Vázquez et al., 2017). We use the following types of data augmentation: (1) image zoom (from 0.9 to 1.1), (2) image random cropping, (3) image rotation (from 0 deg to 180 deg), and (4) image shear (from 0 to 0.4).

Post-processing: As a last stage, we postprocess the resulting segmentation masks aiming to increase the quality of the results. We have tested two specific methods: (1) fill holes in the resulting masks and (2) compute convex hulls of the masks.

4 EXPERIMENTAL SETUP

We next describe the experimental setup used to train and validate the FCN model. This consists of metrics used for quality measurement (Sec. 4.1) and datasets used for training and testing (Sec. 4.2). As mentioned before, we address the problem of polyp characterization as a segmentation problem, since segmentation also gives information about the shape of a polyp. Hence, our model outputs a binary segmentation mask. From this mask, we derive polyp detection and localization.

4.1 Performance Metrics

We evaluate polyp segmentation using the Jaccard index (Vázquez et al., 2017) and the Sörensen-Dice coefficient (Vázquez et al., 2017). With respect to polyp detection and localization, we follow the guidelines in (Bernal et al., 2017): We compare the output of the segmentation to the ground truth (labeled image): For detection, we only care about the presence of a mask in the ground truth to account for frame-based metrics. For polyp localization, we also consider the position of the output. A true positive in polyp detection occurs when the segmentation output overlaps with the ground-truth mask. A true positive in polyp localization occurs when the centroid of the output segmentation mask should falls within the ground-truth mask. It is worth to mention that only one true positive is accounted for each polyp, whereas many false positives can appear in a single image. Once frame-based metrics are defined, we can easily calculate aggregated metrics such as Precision, Recall, Specificity, Accuracy, and F-scores.

4.2 Datasets

We employ two criteria when considering the use of a specific dataset for training/validation: (1) the dataset should be publicly available and (2) the dataset should have been properly annotated. Considering this, we use in our experiments several public datasets that have been presented in the context of MICCAI challenges on Automatic Polyp Detection and Gastrointestinal Image Analysis. For standard definition (SD) images, we use the CVC-EndosceneStill dataset (Vázquez et al., 2017) for still frame analysis. With respect to video analyis, we use the training subset of CVC-VideoClinicDB (Bernal et al., 2018) for network training and the first 9 videos of the testing set using the results provided by the online evaluation tool prepared by challenger organizers. For high definition (HD) images, we use the ETIS-Larib dataset (Bernal et al., 2017). It has to be noted that, in the CVC-VideoClinicDB dataset, the ground truth represents an *approximation* of the polyp in the image using ellipses. Given this, the model trained by this dataset is evaluated against detection and localization metrics instead of segmentation ones.

5 RESULTS

5.1 Polyp Segmentation

Table 4 overviews our experiments regarding polyp segmentation. They consist of four experiments (1..4). In each one, a different database is used for training the network. In all experiments, we use 80% of the dataset for training, and the remaining 20% for validation. Note that the ETIS-Larib database is used in two different ways: For experiment 1.2, we use the original images. For experiment 2, we resize these to 50% while keeping the aspect ratio. This resizing is performed aiming to avoid impact of image resolution differences in method performance.

Figure 2 shows various resulting segmentations given by the trained model. As visible, polyps of quite different shapes, locations, orientations, colors, and lighting are segmented well.

Figure 3 shows the Jaccard index boxplots for experiments 1.1 and 2. We can infer that resizing has a significant influence on the segmentation mask quality, as the resulting Jaccard index seems to be significantly higher than of the original size dataset. The DICE coefficient follows the same trend. It should be noted, however, that the standard deviation of the resized results is also higher. This is probably due to the fact that the network is trained with SD data, whereas the testing HD data captures more texture, which might interfere with the resulting segmentation.

Table 6 shows the overall localization results for each applied post-processing method. We can observe that the selection of the largest blob leads to a significant improvement in precision and specificity, for the paid price of a small decrease in recall results.

The input dataset is preprocessed in Experiment 2, by a filter that enhance the image quality by removing specular highlights. (Sánchez et al., 2017). As Figure 3 shows, it seems that this has a slight impact on the quality of the final segmentation mask. In this case, performance on the preprocessed dataset is slightly lower than in the original one.

5.2 Polyp Detection and Localization

For polyp detection and localization we consider the following three types of result mask post-processing: (1) no post-processing, (2) small morphological opening to remove small-scale noise, and (3) selection of the largest connected component. Table 5 shows the overall detection results for each applied post-processing method. From this, we can see that the small opening leads to a slight improvement in precision, specificity, and mean reaction time, and a small decrease in recall and accuracy.

It is difficult to put these results in the context of other methods, as quantitative results and full datasets of GIANA 2017 and 2018 challenges are not public

Table 4: Experiments and results of polyp segmentation (Sec. 5.1).

Exp.	Database	Training & Validation	Testing	Post-processing	Jaccard		Dice	
					Mean	std	Mean	std
1.1	CVC-EndoSceneStill	612	300	None	0.5819	0.2727	0.6905	0.2678
				Fill holes	**0.5820**	0.2727	**0.6906**	0.2678
				Convex hull	0.5798	0.2733	0.6884	0.2692
1.2	CVC-EndoSceneStill ETIS-Larib	612 -	- 196	None	**0.2258**	0.2111	**0.3230**	0.2672
				Fill holes	0.2257	0.2111	0.3228	0.2672
				Convex hull	0.2250	0.2171	0.3198	0.2717
2	CVC-EndoSceneStill Resized ETIS-Larib	612 -	- 196	None	0.3694	0.3214	0.4579	0.3536
				Fill holes	0.3695	0.3215	0.4579	0.3537
				Convex hull	**0.3759**	0.3284	**0.4623**	0.3584
3	CVC-EndoSceneStill	300	612	None	0.4670	0.2889	0.5754	0.3153
				Fill holes	0.4671	0.2890	0.5756	0.3154
				Convex hull	**0.4782**	0.2922	**0.5853**	0.3172
4	CVC–EndoSceneStill (preprocessed)	612	300	None	0.5635	0.2631	0.6786	0.2559
				Fill holes	**0.5635**	0.2631	**0.6787**	0.2558
				Convex hull	0.5561	0.2658	0.6713	0.2597

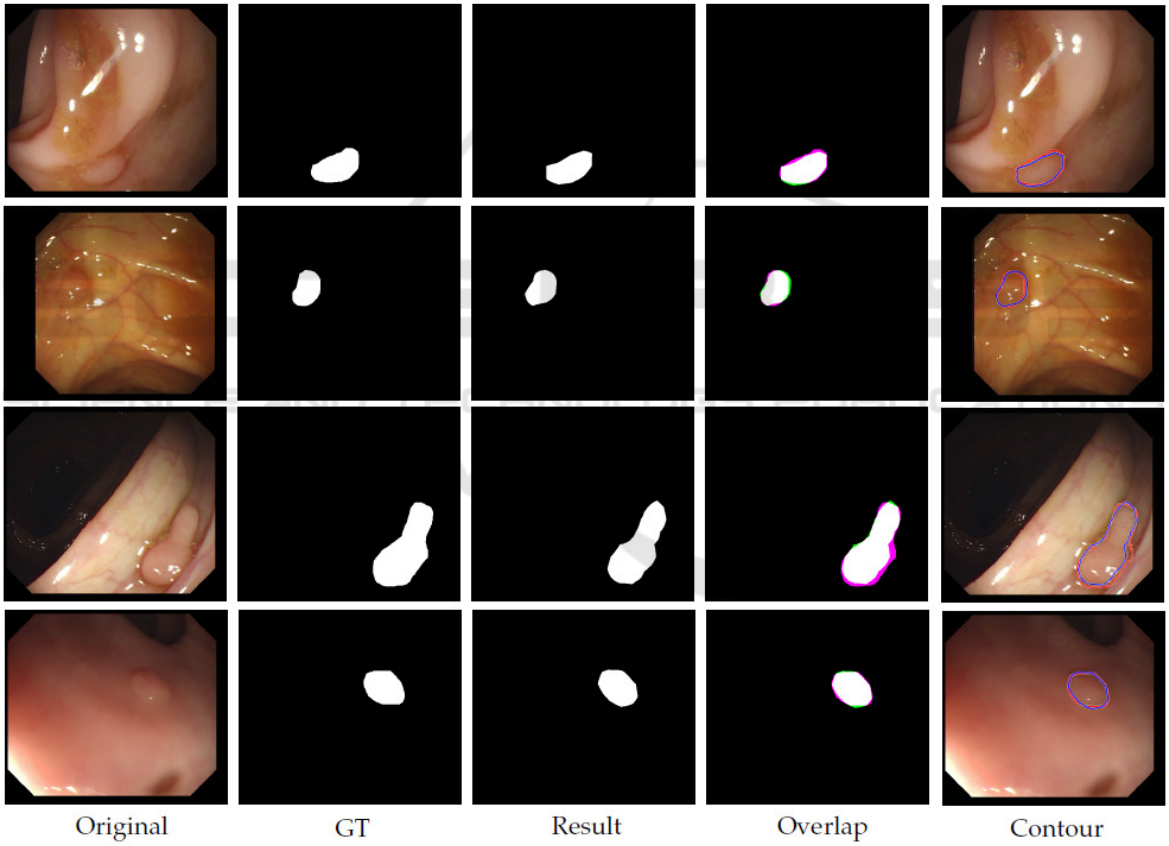

Figure 2: Examples of resulting segmentations. **Original** = Original input image. **GT** = Ground-truth image. **Result** = Resulting image. **Overlap** = Overlap between GT and Result with overlapping pixels between GT and Result in white; pixels in GT but not in Result in magenta (true positives); and pixels in Result but not in GT in green (false positives). **Contour** = Boundaries of the GT (red) and Result (blue) on the original image.

yet and there are not other fully publicly available datasets. Nevertheless, current performance shows the ability of the proposed configuration to detect all different polyps, regardless of their size and appearance. Moreover, the use of computationally-light post processing methods show a significant improvement with respect to the reduction of false alarms, specially for the case of polyp localization.

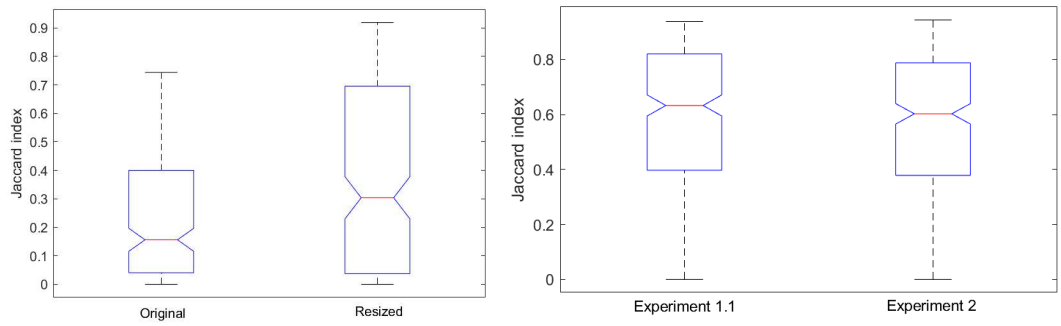

(a) experiment 1.2, original size and resized (b) experiment 1.1 and experiment 2

Figure 3: Boxplots: Jaccard index for (a) experiments 1.2 (original images against resized images) and (b) 2 and Experiment 1.1 against experiment 2.

Table 5: Summary of resulting metrics for detection, for each post-processing method: True positives (TP), false positives (FP), true negatives (TN), false negatives (FN), precision (PR), recall (REC), specificity (SP), accuracy (ACC), and mean response time (RT).

Post-processing	**TP**	**FP**	**TN**	**FN**	**PR**	**REC**	**SP**	**ACC**	**RT**
No post-processing	**4366**	485	2879	**2189**	90.00	**66.60**	85.58	**73.04**	**33.11**
Small opening	4315	**465**	**2899**	2240	**90.27**	65.82	**86.17**	72.79	33.11

Table 6: Summary of resulting metrics for localization for each post-processing method. See Tab. 5 for legend.

Post-processing	**TP**	**FP**	**TN**	**FN**	**PR**	**REC**	**SP**	**ACC**	**RT**
No post-processing	**3953**	1317	2879	**2602**	75.00	60.30	68.61	63.54	34.77
Small opening	3916	1225	2899	2639	76.17	59.74	70.29	63.81	33.66
Largest blob	3876	**904**	**2899**	2679	**81.08**	**59.13**	**76.22**	**65.40**	**33.66**

6 DISCUSSION

We have shown how our methodology is able to provide good results for all the three tasks that have been targeted. Several observations follow. We can see that specific aspects of the different datasets being used can visibly affect the obtained results. For video sequences, the lack of precisely annotated data has impacted the performance of our method, as it is asked to provide an accurate pixel-wise segmentation while it is trained with some pixels that actually do not belong to the polyp class. We predict that having pixel-wise masks for the video dataset could lead to an improvement in performance.

Performance metrics alone do not represent the actual usefulness of a given system in a clinical environment. Apart from frame-based metrics, we should also consider the feasibility of our solution in both technical and clinical contexts. Our proposed network was trained and executed during inference on an Intel Core i7 PC at 2.60GHz having a NVIDIA GeForce GTX 960m GPU card with 2 GB RAM. This is a reasonably affordable platform that could be deployed in clinical practice at a relatively low cost.

In order for a detection method to be used in the exploration room, it should process images in real-time so the exploration is not delayed. Considering that videos are recorded at 25 fps, processing time should not exceed 40 ms. Table 7 shows the average computational time in milliseconds for inferring a single image on a trained model. As visible, the current results are still slower than the 40 ms target. However, we should note that, for HD images, if we are seeking for a posterior in-vivo histology prediction, real-time requirements could be relaxed. Separately, we note that typical year-over-year performance increases of GPUs will actually bring the computation time of SD images well within the target range within likely one year, without increasing the GPU price range.

Table 7: Average computation time (ms).

Image type	**Average computation time (ms)**
Standard Definition (SD)	125
High Definition (HD)	905

With respect to clinical constraints, the most important metric here is the *mean reaction time* (RT), *i.e.*, the number of frames the method needs to accu-

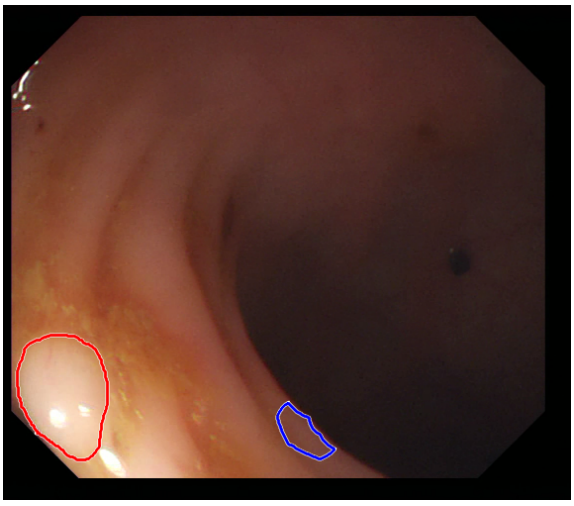

Figure 4: An example of FP and FN result. Red shows the (missed, FN) ground truth and blue shows our FP result.

rately detect a polyp. In our experiments, our method achieves a RT of 33.11 frames for detection and a RT of 33.66 seconds for localization, respectively (Tables 5 and 5). Good RT values in clinical practice should range around one second, so the tool's response is perceived as instantaneous. Our current results are a little over a second though it has to be noted that, for 7 out of 9 videos, RT is of 0 frames. Mean RT is damaged by one specific video with a RT of 298 frames so, for the majority of the videos, the method provides an instantaneous response.

6.1 Limitations

Figure 4 shows an example of a FP and a FN result. Currently, it is hard to tell what is the reason behind the appearance of such results, apart from the obvious observation that, for FNs, there are polyps whose appearance, under the given lighting conditions, is very similar to healthy surrounding gastrointestinal skin texture. Concerning both FP and FN results, we believe that these can be improved by using a larger and more diverse training set, as typical in deep learning.

7 CONCLUSIONS

Several computational methods for polyp characterization in colonoscopy have been proposed but, to the best of our knowledge, none of them tackles the complete polyp characterization task using the same methodology. We have presented in this paper a first approach to polyp characterization using a single methodology, encoded by a single neural network architecture (ResNet50).

We have tested our method on several public available datasets. Results shows that our method can detect and locate various types of polyps appearing in various types of input imagery, providing accurate segmentation masks, especially when the method is tested in still frames. Nevertheless, the actual configuration of our method does not comply with the technical constraints needed for an efficient deployment in the exploration room. Efforts should be undertaken to decrease processing time while keeping, and ideally increasing, performance levels.

One of the reasons of the slightly lower performance of segmentation network in video sequences is the lack of pixel-wise masks for the available datasets. Additional annotations might be gathered to improve this data, which could also lead to an improvement of the performance of the proposed method.

REFERENCES

Alexandre, L. A., Casteleiro, J., and Nobreinst, N. (2007). Polyp detection in endoscopic video using svms. In *European Conference on Principles of Data Mining and Knowledge Discovery*, pages 358–365. Springer.

Alexandre, L. A., Nobre, N., and Casteleiro, J. (2008). Color and position versus texture features for endoscopic polyp detection. In *BioMedical Engineering and Informatics, 2008. BMEI 2008. International Conference on*, volume 2, pages 38–42. IEEE.

Bernal, J., Histace, A., Masana, M., Angermann, Q., Sánchez-Montes, C., Rodriguez, C., Hammami, M., Garcia-Rodriguez, A., Córdova, H., Romain, O., et al. (2018). Polyp detection benchmark in colonoscopy videos using gtcreator: A novel fully configurable tool for easy and fast annotation of image databases. In *Proceedings of 32nd CARS conference*.

Bernal, J., Sánchez, F. J., Fernández-Esparrach, G., Gil, D., Rodríguez, C., and Vilariño, F. (2015). Wm-dova maps for accurate polyp highlighting in colonoscopy: Validation vs. saliency maps from physicians. *Computerized Medical Imaging and Graphics*, 43:99–111.

Bernal, J., Tajkbaksh, N., Sánchez, F. J., Matuszewski, B. J., Chen, H., Yu, L., Angermann, Q., Romain, O., Rustad, B., Balasingham, I., et al. (2017). comparative validation of polyp detection methods in video colonoscopy: results from the miccai 2015 endoscopic vision challenge. *IEEE transactions on medical imaging*, 36(6):1231–1249.

Brandao, P., Mazomenos, E., Ciuti, G., Caliò, R., Bianchi, F., Menciassi, A., Dario, P., Koulaouzidis, A., Arezzo, A., and Stoyanov, D. (2017). Fully convolutional neural networks for polyp segmentation in colonoscopy. In *Medical Imaging 2017: Computer-Aided Diagnosis*, volume 10134, page 101340F. International Society for Optics and Photonics.

Dhandra, B. V., Hegadi, R., Hangarge, M., and Malemath, V. S. (2006). Analysis of abnormality in endoscopic images using combined hsi color space and watershed segmentation. In *Pattern Recognition, 2006. ICPR 2006. 18th International Conference on*, volume 4, pages 695–698. IEEE.

Eskandari, H., Talebpour, A., Alizadeh, M., and Soltanian-Zadeh, H. (2012). Polyp detection in wireless capsule endoscopy images by using region-based active contour model. In *Biomedical Engineering (ICBME), 2012 19th Iranian Conference of*, pages 305–308. IEEE.

Ganz, M., Yang, X., and Slabaugh, G. (2012). Automatic segmentation of polyps in colonoscopic narrow-band imaging data. *IEEE Transactions on Biomedical Engineering*, 59(8):2144–2151.

He, K., Zhang, X., Ren, S., and Sun, J. (2016). Deep residual learning for image recognition. In *Proceedings of the IEEE conference on computer vision and pattern recognition*, pages 770–778.

Hwang, S. and Celebi, M. E. (2010). Polyp detection in wireless capsule endoscopy videos based on image segmentation and geometric feature. In *Acoustics Speech and Signal Processing (ICASSP), 2010 IEEE International Conference on*, pages 678–681. IEEE.

Hwang, S., Oh, J., Tavanapong, W., Wong, J., and De Groen, P. C. (2007). Polyp detection in colonoscopy video using elliptical shape feature. In *Image Processing, 2007. ICIP 2007. IEEE International Conference on*, volume 2, pages II–465. IEEE.

Iakovidis, D. K. and Koulaouzidis, A. (2014). Automatic lesion detection in wireless capsule endoscopy—a simple solution for a complex problem. In *Image Processing (ICIP), 2014 IEEE International Conference on*, pages 2236–2240. IEEE.

Iakovidis, D. K., Maroulis, D. E., Karkanis, S. A., and Brokos, A. (2005). A comparative study of texture features for the discrimination of gastric polyps in endoscopic video. In *Computer-Based Medical Systems, 2005. Proceedings. 18th IEEE Symposium on*, pages 575–580. IEEE.

Karargyris, A. and Bourbakis, N. (2009). Identification of polyps in wireless capsule endoscopy videos using log gabor filters. In *Life Science Systems and Applications Workshop, 2009. LiSSA 2009. IEEE/NIH*, pages 143–147. IEEE.

Karkanis, S. A., Iakovidis, D. K., Maroulis, D. E., Karras, D. A., and Tzivras, M. (2003). Computer-aided tumor detection in endoscopic video using color wavelet features. *IEEE transactions on information technology in biomedicine*, 7(3):141–152.

Kingma, D. P. and Ba, J. (2014). Adam: A method for stochastic optimization. *arXiv preprint arXiv:1412.6980*.

Leufkens, A., van Oijen, M., Vleggaar, F., and Siersema, P. (2012). Factors influencing the miss rate of polyps in a back-to-back colonoscopy study. *Endoscopy*, 44(05):470–475.

Magoulas, G. D., Plagianakos, V. P., and Vrahatis, M. N. (2004). Neural network-based colonoscopic diagnosis using on-line learning and differential evolution. *Applied Soft Computing*, 4(4):369–379.

Mamonov, A. V., Figueiredo, I. N., Figueiredo, P. N., and Tsai, Y.-H. R. (2014). Automated polyp detection in colon capsule endoscopy. *IEEE transactions on medical imaging*, 33(7):1488–1502.

Maroulis, D. E., Iakovidis, D. K., Karkanis, S. A., and Karras, D. A. (2003). Cold: a versatile detection system for colorectal lesions in endoscopy video-frames. *Computer Methods and Programs in Biomedicine*, 70(2):151–166.

Park, S. Y., Sargent, D., Spofford, I., Vosburgh, K. G., Yousif, A., et al. (2012). A colon video analysis framework for polyp detection. *IEEE Transactions on Biomedical Engineering*, 59(5):1408–1418.

Rabeneck, L., El-Serag, H. B., Davila, J. A., and Sandler, R. S. (2003). Ooutcomes of colorectal cancer in the united states: No change in survival (1986–1997). *The American journal of gastroenterology*, 98(2):471.

Ratheesh, A., Soman, P., Nair, M. R., Devika, R., and Aneesh, R. (2016). Advanced algorithm for polyp detection using depth segmentation in colon endoscopy. In *Communication Systems and Networks (ComNet), International Conference on*, pages 179–183. IEEE.

Sánchez, F. J., Bernal, J., Sánchez-Montes, C., de Miguel, C. R., and Fernández-Esparrach, G. (2017). Bright spot regions segmentation and classification for specular highlights detection in colonoscopy videos. *Machine Vision and Applications*, 28(8):917–936.

Siegel, R. L., Miller, K. D., Fedewa, S. A., Ahnen, D. J., Meester, R. G., Barzi, A., and Jemal, A. (2017). Colorectal cancer statistics, 2017. *CA: a cancer journal for clinicians*, 67(3):177–193.

Silva, J., Histace, A., Romain, O., Dray, X., and Granado, B. (2014). Toward embedded detection of polyps in wce images for early diagnosis of colorectal cancer. *International Journal of Computer Assisted Radiology and Surgery*, 9(2):283–293.

Tajbakhsh, N., Gurudu, S. R., and Liang, J. (2014). Automatic polyp detection using global geometric constraints and local intensity variation patterns. In *International Conference on Medical Image Computing and Computer-Assisted Intervention*, pages 179–187. Springer.

Tajbakhsh, N., Gurudu, S. R., and Liang, J. (2015). Automatic polyp detection in colonoscopy videos using an ensemble of convolutional neural networks. In *Biomedical Imaging (ISBI), 2015 IEEE 12th International Symposium on*, pages 79–83. IEEE.

Tajbakhsh, N., Gurudu, S. R., and Liang, J. (2016). Automated polyp detection in colonoscopy videos using shape and context information. *IEEE transactions on medical imaging*, 35(2):630–644.

Tarik, G., Khalid, A., Jamal, K., and Benajah, D. A. (2016). Polyps's region of interest detection in colonoscopy images by using clustering segmentation and region growing. In *Information Science and Technology (CiSt), 2016 4th IEEE International Colloquium on*, pages 455–459. IEEE.

Tjoa, M. P. and Krishnan, S. M. (2003). Feature extraction for the analysis of colon status from the endoscopic images. *BioMedical Engineering OnLine*, 2(1):9.

Vázquez, D., Bernal, J., Sánchez, F. J., Fernández-Esparrach, G., López, A. M., Romero, A., Drozdzal, M., and Courville, A. (2017). A benchmark for endoluminal scene segmentation of colonoscopy images. *Journal of healthcare engineering*, 2017.

Wang, Y., Tavanapong, W., Wong, J., Oh, J., and De Groen, P. C. (2014). Part-based multiderivative edge cross-sectional profiles for polyp detection in colonoscopy. *IEEE Journal of Biomedical and Health Informatics*, 18(4):1379–1389.

Yu, L., Chen, H., Dou, Q., Qin, J., and Heng, P. A. (2017). Integrating online and offline three-dimensional deep learning for automated polyp detection in colonoscopy videos. *IEEE journal of biomedical and health informatics*, 21(1):65–75.

Zhou, M., Bao, G., Geng, Y., Alkandari, B., and Li, X. (2014). Polyp detection and radius measurement in small intestine using video capsule endoscopy. In *Biomedical Engineering and Informatics (BMEI), 2014 7th International Conference on*, pages 237–241. IEEE.